agriculture

MDPI

*Article*

# Pitch Angle Compensation and System Design for Tillage Depth Monitoring of Mounted Moldboard Plough

**Bingbo Cui [1,2,*], Zhihan Hu [1,2], Zelong Yu [1,2], Yongyun Zhu [1,2] and Zhen Ma [1,2]**

[1] Key Laboratory of Modern Agricultural Equipment and Technology, Jiangsu University, Ministry of Education, Zhenjiang 212013, China; 2212516016@stmail.ujs.edu.cn (Z.H.); 2212316044@stmail.ujs.edu.cn (Z.Y.); yongyunzhu@ujs.edu.cn (Y.Z.); 1000005769@ujs.edu.cn (Z.M.)
[2] School of Agriculture Engineering, Jiangsu University, Zhenjiang 212013, China
* Correspondence: cuibingbo@ujs.edu.cn

## Abstract

Ploughing constitutes a fundamental tillage practice for enhancing soil fertility as well as water and fertilizer utilization efficiency. The uniformity of tillage depth directly determines seedling emergence consistency and final crop yield. Conventional indirect tillage depth detection approaches based solely on the rotation angle of the tractor lift arm are susceptible to disturbances induced by uneven terrain and dynamic attitude fluctuations of the tractor-implement system. To compensate for disturbances induced by tractor pitch angle variations, existing pitch compensation models adopt cascaded output compensation to calculate tillage depth. Nevertheless, these models need recalibration after each modification to the three-point hitch linkage length and are incapable of simultaneously compensating for pitch variations in the tractor and attached implement. To reduce the sensitivity of the tillage depth model to structural changes in the three-point hitch, this work constructs a mapping between hitch structural geometric deviations and vertical projection offsets of key linkages via tractor–plough integrated distributed attitude sensing. In this paper, a distributed tillage depth model is developed, which takes the distributed attitude of the whole working unit and the pitch of the lower-link measured by a rotation angle sensor as independent input variables. Field validation was performed with a mounted moldboard plough, with ultrasonic ranging sensor tillage depth readings serving as the reference benchmark to assess the reliability and precision of the proposed distributed model. Experimental results show that compared with the pitch angle cascaded tillage depth model, the average root mean square error of the proposed method is reduced from 22.5 mm to 12.5 mm on bumpy fields and from 11.3 mm to 8.7 mm on flat fields. The distributed model can significantly improve the measurement accuracy and anti-interference capability of tillage depth detection on uneven farmland, and it is applicable to adaptive measurement and control of tillage depth in complex ploughing scenarios.

**Keywords:** tractor-mounted unit; moldboard plough; three-point hitch; tillage depth detection; distributed attitude measurement; pitch angle compensation

Check for updates

Academic Editor: Jin He

Received: 18 June 2026
Revised: 23 July 2026
Accepted: 23 July 2026
Published: 26 July 2026

**Copyright:** © 2026 by the authors. Licensee MDPI, Basel, Switzerland. This article is an open access article distributed under the terms and conditions of the Creative Commons Attribution (CC BY) license.

## 1. Introduction

Tractor ploughing serves as an essential practice to break up plough pans, retain soil water, and preserve soil moisture. The tillage depth uniformity coefficient is a key agronomic parameter that influences seedling emergence uniformity, soil compaction, crop yield, and tractor powertrain design [1–4]. Researchers have extensively studied the

factors affecting the stability of tillage depth detection and control models under various tillage scenarios [5–7]. Growing adoption of intelligent agricultural control systems, such as precision seedbed preparation [8–10], tractor trajectory tracking [11], and tillage depth control accounting for engine load variations [12,13], poses new challenges to high-precision tillage depth sensing.

Existing tillage depth detection methods primarily include indirect measurement via angle detection, ground profiling measurement, and direct detection based on ranging sensors [14–16]. Most of these methods develop tillage depth detection systems tailored to specific application scenarios and farm implements, yet their adaptability across various working conditions and the generalizability of the corresponding algorithmic models require further investigation. Jia et al. designed an adaptive tillage depth monitoring system according to the pitch angle between the implement and ground, and the inclined angle of the ground [17]. Kim et al. implemented tillage depth detection by installing a gauge wheel at their self-developed tractor-implement three-point hitch mechanism, in combination with a displacement sensor [18]. Soylu et al. implemented tillage depth detection by attaching a depth-measuring gauge wheel at the rear end of the plough frame, in combination with a rotary potentiometer placed at its center of rotation [19]. Sukcharoenvipharat et al. developed a system for simultaneously measuring soil strength and subsoiling depth. The system calculates the relative distance between the tillage implement and soil surface using an ultrasonic sensor fixed to the subsoiler frame [20]. In order to compensate for the effect of an uneven surface for subsoiling, Lou et al. developed an independent adjustment system for each subsoiling shovel to be controlled separately, where the ultrasonic sensor was employed to detect the tillage depth of each subsoiling shovel [21]. Wang et al. developed a tillage depth control system based on real-time tillage depth feedback, where the mechanical angle sensor and inertial measurement unit (IMU) were utilized to construct the tillage depth model [22]. The stability of the aforementioned tillage depth model is susceptible to ground flatness, working unit vibration, and the dynamic precision of attitude sensors.

Indirect tillage depth detection models built upon lift arm angle changes eliminate issues arising from profiling mechanism structural deformation and surface crop residue interference, rendering them extensively adopted for tillage depth sensing and control of mounted agricultural implements. To further improve the scenario adaptability of tillage depth models, Ma et al. designed a profiling mechanism to detect pre-operation terrain features and tractor sinkage to compensate for the tillage depth detection model [23]. To reduce the impact of ground stubble on ranging-based tillage depth detection, Jiang et al. combined ultrasonic sensors and infrared sensors for tillage depth detection and processed the data using a Kalman fusion algorithm [24]. Du et al. utilized inertial sensors to collect the horizontal inclination angles of the lower link and the rotary tiller frame, achieving nonlinear tillage depth detection in shallow tillage scenarios [25]. Yin et al. installed attitude sensors on the rear suspension rod and the frame of a subsoiler to detect their angles relative to the horizontal ground [26]. The aforementioned methods are suitable for flat-ground tillage operations but do not consider the impact of the pitch angles of the tractor and implement on tillage depth detection during actual operations. To mitigate the influence of surface evenness on tillage depth control, Xia et al. employed an angular displacement sensor and an inclination sensor to detect the lift arm rotation and the tractor pitch, feeding the tillage depth error caused by vehicle body pitch changes back into the depth control loop [27]. This method relies on a specific three-point hitch structure, and the attitude compensation term calibrated on this basis is easily affected by adjustments to the hitch structure. Hu et al. developed a piecewise linear tillage depth model with a hydraulic cylinder stroke and tractor pitch angle as input variables, enhancing both tillage depth

detection precision and control performance [28]. Such methods depend on the installation precision of the hydraulic cylinder, and the piecewise model not only introduces switching errors but also increases the model calibration workload.

To solve the aforementioned problems, this work proposes an improved indirect tillage depth detection method based on distributed pitch angle monitoring of the tractor and plough. After analyzing the influencing factors of the tillage depth model, length variations in the three-point linkage and tractor rear wheel sinkage are translated into quantified relative pitch shifts between the tractor and plough. We then establish a distributed tillage depth model, where the distributed tillage unit attitude and lift arm rotation angle serve as independent variables, and real-time tillage depth acts as the dependent variable. A tillage depth monitoring system matching the mounted moldboard plough is developed, and field tests are implemented on flat and bumpy farmland to verify the efficacy of the proposed method. Experiments are carried out on a Dongfanghong 1104 tractor (YTO Group Corporation, Luoyang, China). It should be noted that during field operations, tractor pitching causes uneven depth variations across the plough frame, which is scaled by the plough length. In this work, the proposed system focuses on dynamic depth tracking at the rearmost ploughshare tip (Point H). With well-tuned plough settings, Point H marks the deepest penetration point of the entire implement. Since this location is most vulnerable to pitch interference, it serves as an essential benchmark to evaluate tillage depth consistency.

## 2. Materials and Methods

### *2.1. Design of Tillage Depth Monitoring System*

To realize real-time tillage-depth detection based on attitude compensation and to validate the effectiveness of the proposed detection method, a tillage-depth monitoring system was developed in this study. The experimental platform of the system is shown in Figure 1. The tractor used in the experiment was a Dongfanghong 1104, the parameters of which are listed in Table 1. The mounted plough was a DZ430 moldboard plough manufactured by Huaian Tieniu Equipment Co., Ltd (Huaian, China), the parameters of which are listed in Table 2. There are two IMUs installed on the tractor body and the plough, respectively, as well as a contact-type angle sensor mounted on the upper lift arm. The tractor-mounted IMU was installed horizontally on the cab floor, while the plough-mounted IMU was installed on the horizontal section of the plough frame. Since the IMUs are adopted to measure the attitude variations in the tractor and plough, their mounting positions are arranged close to the origin of the carrier coordinate systems of the tractor and plough, respectively. The contact-type angle sensor was used to acquire digital sampling values for calculating the pitch angle of the lower link. The angle sensor used in the system was the original factory-installed sensor of the tractor, and the IMU model was the RION HDA437(Shenzhen Ruifen Technology Co. Ltd., Shenzhen, China). Its main specifications are listed in Table 3. Levelness tests were conducted on both level ground and a raised platform during plough installation. By iteratively adjusting the three-point hitch linkage lengths, the plough was kept horizontal to maintain consistent working depths across all four plough bodies.

The software workflow for tillage depth detection is shown in Figure 2. The tillage depth monitoring system is developed using the Qt framework (Version 5.14.2) to enable real-time tillage depth monitoring and data visualization, with a depth data update frequency of 5 Hz. An STM32F107 series microcontroller is employed to acquire data from the angle sensor and IMUs. A timer interrupt triggers periodic sampling at 100 Hz. The microcontroller collects six-axis IMU data from both the tractor and plough, combines it with the angle sensor readings, and transmits the dataset to the host computer in a predefined format. After the program is initialized, data from both IMUs and the angle sensor are

acquired. The IMU raw data of the tractor and plough are processed using a robust Kalman filter (RKF) given in the next section to estimate the attitudes of the tractor and plough, respectively. Meanwhile, the digital sampling values from the angle sensor are resolved through the lower-link angle model to obtain the pitch of the lower link. Subsequently, the obtained attitude information is input into the distributed tillage depth model to calculate the tillage depth, which is then displayed online in the monitoring interface.

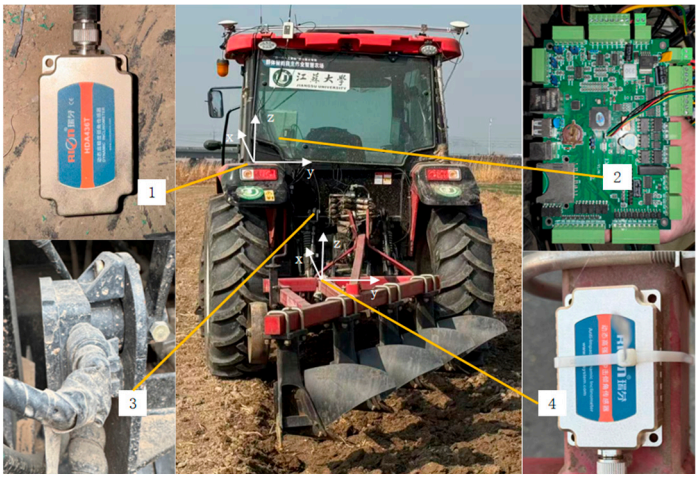



**Figure 1.** Test platform for tillage depth monitoring system. 1. Tractor-mounted IMU; 2. industrial control board; 3. angle sensor; 4. And plough-mounted IMU.

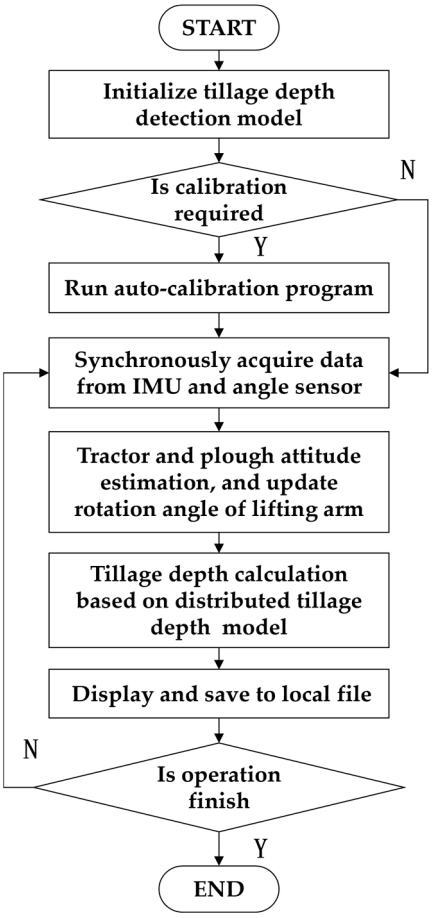



**Figure 2.** The flowchart of distributed tillage depth detection.

**Table 1.** Parameters of Dongfanghong 1104.

| Parameter | Value |
|---|---|
| Length × Width × Height (mm × mm × mm) | 4436 × 2250 × 2765 |
| Ground clearance (mm) | 440 |
| Hitch height (mm) | 580 |
| Working speed (km/h) | 2.69–37.65 |
| Minimum turning radius (m) | 5.6 |
| Front wheel thread (mm) | 1760 |
| Rear wheel thread (mm) | 1820 |
| Wheel base length (mm) | 2314 |
| Front tread width (mm) | 1748 |
| Rear tread width (mm) | 1620 |
| Three-point hitch category | Category II |
| Draw bar power (kw) | 48.6 |
| Engine power (kw) | 81 |

**Table 2.** Parameters of DZ430 moldboard plough.

| Parameter | Value |
|---|---|
| Bottoms | 4 |
| Single bottom width (mm) | 300 |
| Hitch category | Category II |
| Total longitudinal length (mm) | 2685 |

**Table 3.** Performance indicators of the IMU.

| Sensors | Parameter | Value |
|---|---|---|
| Gyroscope | Measurement range<br>bias stability | ±250°/s<br>8.5°/h |
| Accelerometer | Measurement range<br>bias stability | ±8 g<br>0.02 mg |

### *2.2. Robust Attitude Estimation Based on IMU*

Precise dynamic attitude estimation of the tractor and plough serves as a prerequisite for establishing the tillage depth model. The IMU used in this study is composed of a triaxial gyroscope and a triaxial accelerometer. Let the gyroscope measurement output at time step $k$ be:

$$\boldsymbol{y}_{w,k} = \boldsymbol{w}_{ib,k}^{b} + \boldsymbol{b}_{w,k} + \boldsymbol{n}_{w,k} \tag{1}$$

where $\boldsymbol{w}_{ib,k}^{b}$ represents the ideal angular velocity, $\boldsymbol{b}_{w,k}$ is the gyroscope bias term, and $\boldsymbol{n}_{w,k}$ is Gaussian white noise. To reduce the impact of random drift on attitude estimation, let $\boldsymbol{w}_{b,k}$ be zero-mean Gaussian white noise, and the gyroscope bias term is modeled as:

$$\boldsymbol{b}_{w,k} = \boldsymbol{b}_{w,k-1} + \boldsymbol{n}_{b,k} \tag{2}$$

The output of the accelerometer at $k$ instant is:

$$\boldsymbol{y}_{a,k} = \boldsymbol{a}_{k} + \boldsymbol{g}^{b} + \boldsymbol{n}_{a,k} \tag{3}$$

where $\boldsymbol{a}_k$ represents external acceleration, $\boldsymbol{g}^b$ is the gravitational acceleration in the vehicle body frame ($b$-frame), and $\boldsymbol{n}_{a,k}$ is Gaussian white noise. Assuming the external acceleration changes slowly, it can be expressed by a first-order low-pass filtered white noise process:

$$\boldsymbol{a}_k = c_a \boldsymbol{a}_{k-1} + \boldsymbol{\varepsilon}_{k-1} \tag{4}$$

where $c_a$ is a constant ranging from 0 to 1, $\boldsymbol{\varepsilon}_{k-1}$ representing the modeling error of the vehicle's accelerated motion. By applying a first-order approximation to solve the direction cosine matrix (DCM) differential equation at time step $k$, we obtain:

$$\boldsymbol{C}_{b,k}^{n} = \boldsymbol{C}_{b,k-1}^{n}\left(\boldsymbol{I}_{3\times 3} + \Delta T\left(\boldsymbol{w}_{ib,k}^{b}\times\right)\right) \tag{5}$$

where $\boldsymbol{w}_{ib,k}^{b}$ denotes the angular rate of the vehicle body with respect to the inertial frame ($i$-frame) and resolved in the $b$-frame. $\left(\boldsymbol{w}_{ib,k}^{b}\times\right)$ denotes the skew-symmetric matrix of the vector $\boldsymbol{w}_{ib,k}^{b}$, and $\Delta T$ is the sampling period of the gyroscope. The navigation frame ($n$-frame) in this work is selected as North-East-Down, and the $b$-frame is selected as Front-Right-Down. From the last row of DCM $z\boldsymbol{C}_{b,k}^{n}$, the roll and pitch can be obtained [26]. Let the attitude state model equation be

$$\boldsymbol{x}_k = \boldsymbol{\Phi}_{k|k-1}\boldsymbol{x}_{k-1} + \boldsymbol{w}_{k-1} \tag{6}$$

Considering the gyroscope bias error, the state vector is chosen as $x_k = \begin{bmatrix} z\boldsymbol{C}_{b,k}^{n} & \boldsymbol{b}_{w,k} \end{bmatrix}^T$. Substituting (1) into (5) yields:

$$\begin{aligned} z\boldsymbol{C}_{b,k}^{n} &= z\boldsymbol{C}_{b,k-1}^{n}\left(\boldsymbol{I}_{3\times 3} + \Delta T\left(\boldsymbol{y}_{w,k} - \boldsymbol{b}_{w,k} - \boldsymbol{n}_{w,k}\right)\times\right) \\ &= \left(\boldsymbol{I}_{3\times 3} - \Delta T\left(\boldsymbol{y}_{w,k}\times\right)\right)z\boldsymbol{C}_{b,k-1}^{n} + \Delta T\left(-z\boldsymbol{C}_{b,k-1}^{n}\times\right)\boldsymbol{b}_{w,k} + \Delta T\left(-z\boldsymbol{C}_{b,k-1}^{n}\times\right)\boldsymbol{n}_{w,k} \end{aligned} \tag{7}$$

Comparing (6) and (7) yields:

$$\boldsymbol{\Phi}_{k|k-1} = \begin{bmatrix} \boldsymbol{I}_{3\times 3} - \Delta T\left(\boldsymbol{y}_{w,k}\times\right) & \Delta T\left(-z\boldsymbol{C}_{b,k-1}^{n}\times\right) \\ \boldsymbol{0}_{3\times 3} & \boldsymbol{I}_{3\times 3} \end{bmatrix} \tag{8a}$$

$$\boldsymbol{w}_{k-1} = \begin{bmatrix} \Delta T\left(-z\boldsymbol{C}_{b,k-1}^{n}\times\right) & \boldsymbol{0}_{3\times 3} \\ \boldsymbol{0}_{3\times 3} & \boldsymbol{I}_{3\times 3} \end{bmatrix}\begin{bmatrix} \boldsymbol{n}_{w,k} \\ \boldsymbol{n}_{b,k} \end{bmatrix} \tag{8b}$$

The system noise covariance matrix is:

$$\boldsymbol{Q}_{k-1} = \begin{bmatrix} \boldsymbol{Q}_{w,k-1} & \boldsymbol{0}_{3\times 3} \\ \boldsymbol{0}_{3\times 3} & \boldsymbol{Q}_{b,k-1} \end{bmatrix} \tag{8c}$$

where $\boldsymbol{Q}_{w,k-1}$ and $\boldsymbol{Q}_{b,k-1}$ correspond to the noise driving matrices of $z\boldsymbol{C}_{b,k}^{n}$ and $\boldsymbol{b}_{w,k}$. Let $\boldsymbol{\Sigma}_{gg} = \mathrm{E}\left[\boldsymbol{n}_{w,k}\boldsymbol{n}_{w,k}^{T}\right]$, where $\mathrm{E}[\cdot]$ denotes the expectation operator, then there is:

$$\boldsymbol{Q}_{w,k-1} = -\Delta T^2\left(z\boldsymbol{C}_{b,k-1}^{n}\times\right)\boldsymbol{\Sigma}_{gg}\left(z\boldsymbol{C}_{b,k-1}^{n}\times\right)^{T} \tag{9}$$

Since $\boldsymbol{g}^{\boldsymbol{b}} = \left(\boldsymbol{C}_{\boldsymbol{b}}^{\boldsymbol{n}}\right)^{\boldsymbol{T}}\boldsymbol{g}^{\boldsymbol{n}} = g_e z\boldsymbol{C}_{b,k-1}^{n}$, combining with (4) yields the accelerometer measurement as:

$$\boldsymbol{y}_{\mathrm{a,k}} - c_{\mathrm{a}}\boldsymbol{a}_{\mathrm{k-1}} = g_{\mathrm{e}} z\boldsymbol{C}_{\mathrm{b,k-1}}^{\mathrm{n}} + \boldsymbol{\varepsilon}_{\mathrm{k-1}} + \boldsymbol{n}_{\mathrm{a,k}} \tag{10}$$

It can be obtained that:

$$z_{\mathrm{k}} = y_{\mathrm{a,k}} - \mathrm{c_a} a_{\mathrm{k-1}} \tag{11a}$$

$$H_k = \begin{bmatrix} g_e I_{1\times 3} & 0_{1\times 3} \end{bmatrix} \tag{11b}$$

$$v_k = \varepsilon_{k-1} + n_{a,k} \tag{11c}$$

Define the innovation as $e_k = z_k - H_k x_k^-$, $x_k^-$ denotes the state prediction. To eliminate the impact of external acceleration on the measurement update, an online estimation model for innovation variance is constructed as follows:

$$C_k = \mathrm{E}\left[e_k e_k^T\right] = H_k P_k^- H_k^T + \Delta\hat{\Sigma}_k + \Sigma_{aa} \tag{12}$$

where the measurement noise variance is $\Sigma_{aa} = \mathrm{E}\left[n_{a,k} n_{a,k}^T\right]$, and the KF gain is:

$$K_k = P_k^- H_k^T \left(H_k P_k^- H_k^T + \Delta\hat{\Sigma}_k + \Sigma_{aa}\right)^{-1} \tag{13}$$

where $P_k^-$ is the state prediction covariance matrix, and $\Delta\hat{\Sigma}_k$ is the variance matrix introduced by external acceleration. When it is detected that the estimated innovation covariance value deviates significantly from the actual measurement, namely:

$$\mathrm{tr}\left(e_k e_k^T\right) > \mathrm{tr}\left(H_k P_k^- H_k^T + \Delta\hat{\Sigma}_k + \Sigma_{aa}\right) \tag{14}$$

the uncertainty in the innovation is compensated, where $\mathrm{tr}(\mathrm{A})$ represents the trace of matrix A. Based on the average value of $C_k$ over multiple time steps to approximate its true value:

$$\hat{C}_k = \frac{1}{\mu}\sum_{j=k-\mu+1}^{k} e_j e_j^T \tag{15}$$

$\mu$ is the length of the innovation sequence. Assuming the deviation between the average variance and the $k$-time-step innovation variance is $\Delta$, then it can be obtained:

$$\Delta = \hat{C}_k - H_k P_k^- H_k^T - \Sigma_{aa} \tag{16}$$

Assuming the vehicle acceleration is mutually independent in the three axes, then there is [29]:

$$\Delta\hat{\Sigma}_k = \mathrm{diag}(s_1, s_2, s_3) \tag{17}$$

where $s_i = \max(0, S_{ii})$, $S_{ii}$ is the $i$ diagonal element of matrix $\Delta$. Based on (8), (11) and the adaptive measurement noise adjustment given in (12)–(17), the dynamic attitude of the plough and tractor can be accurately estimated. Detailed implementation procedures of the RKF are presented in Ref. [30] and its associated references.

### *2.3. Attitude Analysis of the Moldboard Plough*

The side projection of the tractor–plough unit is shown in Figure 3, where the right-hand part represents the tractor body and the left-hand part represents the plough. For modeling purposes, the connecting components are neglected, and the shapes of the linkages are simplified. Accordingly, the hitch system is simplified as a planar linkage structure consisting of the upper lift arm, lift rod, upper link, lower link, and plough frame. In the side projection, the upper lift arm can be represented by link AB, the upper link by link CD, the lower link by link EG, and the lift rod by link AF. Points B, D, and G denote the hinge points on the tractor side, while points C and E denote the hinge points between the hitch linkages and the plough frame. The upper link CD and lower link EG connect the

tractor to the plough frame, thereby constraining the plough attitude. Meanwhile, the lift rod AF connects the upper lift arm to the lower link to transmit rotational motion. Point O denotes the center of the rear wheel axle, and point H denotes the tip of the rearmost ploughshare. When the three-point hitch system is adjusted, the hydraulic cylinder drives the upper lift arm AB to rotate about point B and further drives the lower link EG to rotate, thereby changing the position of the plough and realizing tillage depth adjustment of the moldboard plough.

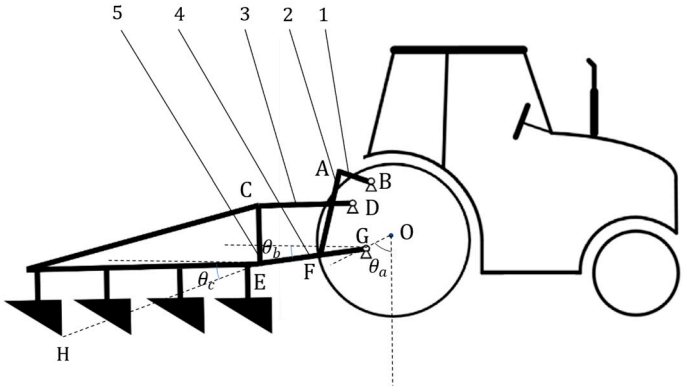



**Figure 3.** Projection of the three-point hitch adjustment process. 1. Upper lift arm; 2. lift rod; 3. upper link; 4. lower link; 5. plough frame.

As the plough is lowered from the highest position to the lowest position, the lift arm rotates from the upper limit position to the lower limit position. Therefore, the tillage depth detection model can be obtained by establishing the corresponding correlation between the upper lift arm angle and the tillage depth. In practical detection, the lift arm angle is acquired and used to calculate the operating tillage depth of the plough. However, the angle-based tillage depth detection model is susceptible to linkage adjustment and implement attitude variation. During the hitching of the moldboard plough and the adjustment of the soil-engaging angle, the length of the upper link needs to be frequently adjusted, and the resulting tillage depth variation is illustrated in Figure 4. When the upper link is extended by $\Delta L$, the plough rotates about hinge point E, and the variation in the plough pitch angle $\Delta\theta_p$ induces a corresponding change in tillage depth $\Delta h$. The tillage depth variation caused by tractor pitch motion is shown in Figure 5. As the tractor body pitches backward by $\Delta\theta_t$ about axle center O, the line segment OH rotates to OH′. This displacement directly induces a tillage depth variation $\Delta h$. These factors alter the original mapping correlation between the lift arm angle and the tillage depth, thereby requiring recalibration of the angle-based tillage depth detection model.

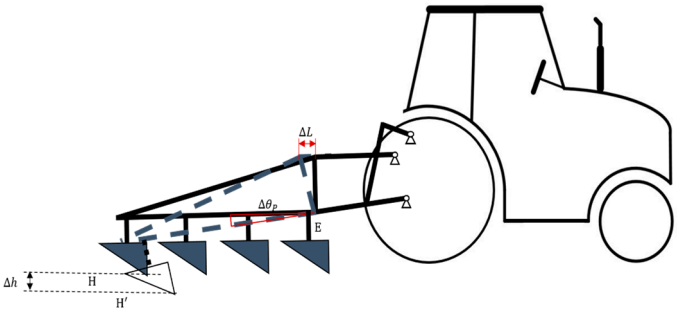



**Figure 4.** Projection of the top link adjustment process.

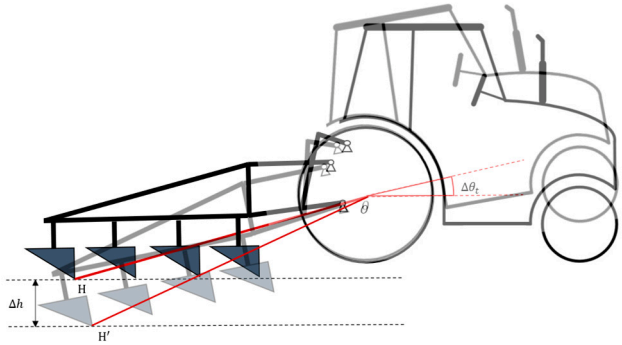



**Figure 5.** Projection of tractor pitch variation.

### *2.4. Influencing Factors Analysis of the Tillage Depth Model*

To analyze the effects of pitch angle variation and linkage length adjustment on the tillage depth detection model, a motion model of a tractor-mounted moldboard plough was established in Solidworks, as shown in Figure 6. Simulation analyses were conducted for the adjustment of the upper-link length and the pitch motion of the tractor. The adjustment of the upper-link length was realized by disconnecting link CD and applying a linear motor, while the tractor pitch motion was simulated by adding a rotary motor about point O. To clarify the influence of each factor on the tillage-depth detection model, the relative angle between the upper lift arm AB and the tractor was kept constant during the simulation.

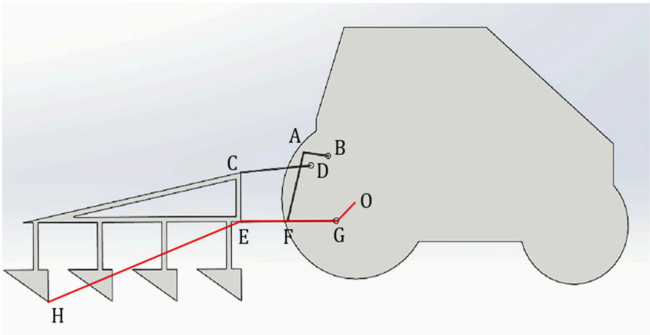



**Figure 6.** Modeling of the moldboard plough unit in Solidworks.

When only the upper-link length was adjusted, the correlations between the length variation in top link $\Delta L$, tillage depth $h$, and plough pitch angle $\theta_p$ are shown in Figure 7. The results indicate that changes in the upper-link length simultaneously alter both the plough pitch angle and the tillage depth, thereby modifying the original calibration correlation between the lift arm angle and the tillage depth. The conventional angle-dependent model is expressed as $h = a\theta_l + b$, where $\theta_l$ denotes the lift arm angle, and $a$ and $b$ represent the gain coefficient and initial offset, respectively. When the upper-link length changes, the model coefficients $a$ and $b$ need to be recalibrated according to the adjusted $\theta_l$ and $h$. When the tractor pitch angle varies, the correlation between the tractor pitch angle $\theta_t$ and tillage depth $h$ is shown in Figure 8, indicating an approximately linear correlation between the tractor body pitch angle and the tillage depth variation.

To compensate for tillage depth deviations induced by tractor pitch, pitch-angle compensation is implemented by cascading a pitch correction term with the angle-based tillage depth detection model [23]. Specifically, $\Delta h = \rho \Delta\theta_t$ is used to correct the tillage depth variation induced by tractor pitch, where $\rho$ represents the tillage depth calibration coefficient corresponding to the change in tractor pitch. This method assumes a fixed mapping correlation between the tractor pitch angle and the tillage depth variation. However, as the lift arm angle changes, the equivalent arm length OH varies accordingly. Consequently, an

identical tractor pitch angle produces inconsistent tillage depth deviations across different hitch states. Therefore, a fixed pitch-angle compensation model is difficult to adapt to different three-point hitch states. After adjustment of the hitch mechanism, parameter a must be recalibrated according to the pitch angle variation and the measured tillage depth deviation under the corresponding hitch state.

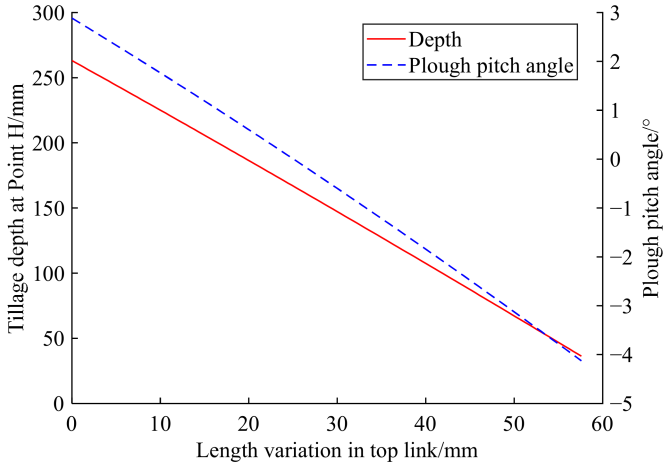



**Figure 7.** Correlation of top-link length variation with tillage depth and implement pitch.

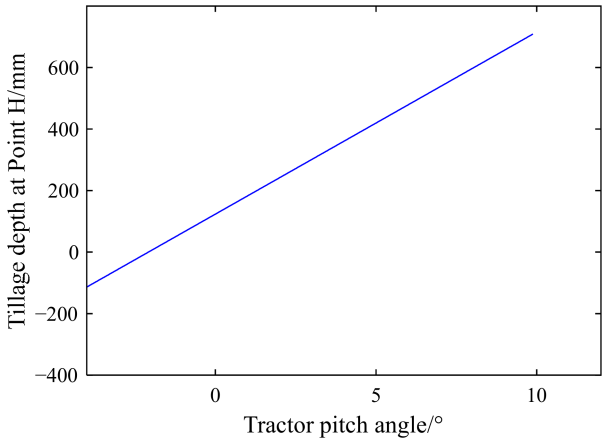



**Figure 8.** Correlation between tractor pitch angle and tillage depth.

### *2.5. Distributed Tillage Depth Model Construction*

To reduce the sensitivity of the tillage depth detection model to adjustments of the three-point hitch structure, a distributed tillage depth model is proposed in this section, in which the distributed attitudes of the tractor–implement unit and the lift arm angle are used as independent variables. In this paper, the upward pitch of the tractor front is defined as positive, and the positive directions of all relevant angles are consistently defined to be the same as that of the tractor pitch angle. The rear three-point hitch and the plough frame shown in Figure 1 are simplified as illustrated in Figure 9. The dashed circle represents the rear wheel of the tractor. Point O denotes the center of the rear wheel axle, and its vertical distance from the ground, $h_o$, is equal to the rear wheel radius. $\theta_a$ and $\theta_c$ are fixed angles determined by the mechanical structure. $\theta_{b0}$ denotes the pitch angle of the lower link relative to the tractor body, $\theta_t$ denotes the tractor body pitch angle, and $\theta_p$ denotes the plough pitch angle.

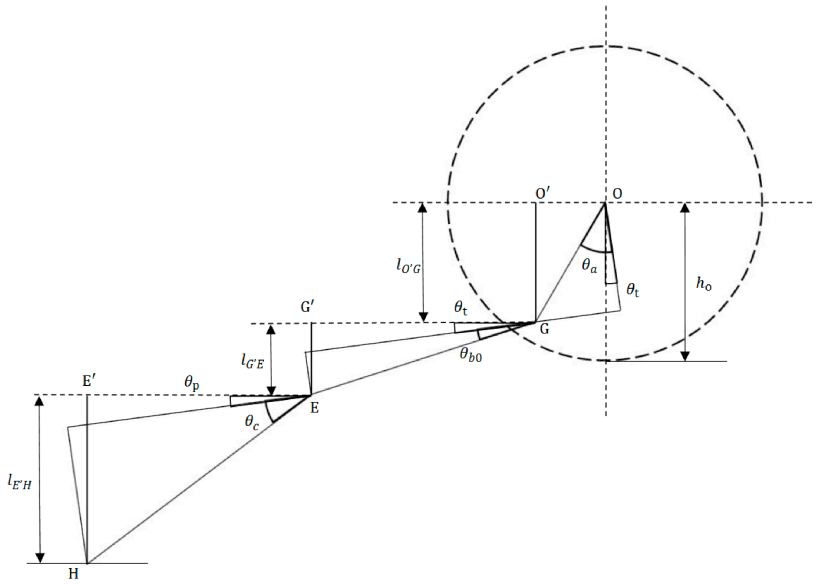



**Figure 9.** Simplification of the tillage depth detection linkage.

Segment EH connects the lower hitch hinge point to the rearmost share tip. Assuming a rigid plough frame, the length of EH remains invariant. O′G, G′E, and E′H denote the vertical projections of OG, GE, and EH, respectively. Therefore, the tillage depth can be expressed as the vertical distance from point O to point H minus the rear wheel radius $h_o$, namely

$$h = l_{O'G} + l_{G'E} + l_{E'H} - h_o \tag{18}$$

where $h$ denotes the tillage depth, $l_{O'G}, l_{G'E}, l_{E'H}$ denote the lengths of O′G, G′E, and E′H, respectively. During field tillage operation, both the plough and the tractor may undergo pitch angle variations. Therefore, the angles used in calculating the projected lengths consist of the fixed angles determined by the mechanical structure and the pitch angles induced by attitude variations. Accordingly, $l_{O'G}$ and $l_{E'H}$ can be expressed as follows:

$$l_{O'G} = l_{OG}cos(\theta_a - \theta_t) \tag{19a}$$

$$l_{E'H} = l_{EH}sin(\theta_c + \theta_p) \tag{19b}$$

where $\theta_t$ denotes the pitch angle of the tractor body; $\theta_p$ denotes the pitch angle of the plough; and $l_{OG}$, $l_{EH}$ denote the lengths of OG and EH, respectively.

The tractor three-point hitch system is equipped with a contact-type lift arm angle sensor, which is installed at the hinge joint between the upper lift arm and the tractor body. The digital sampling values output by this sensor can reflect variations in the three-point hitch configuration. Therefore, the correlation between the sensor output and the lower-link angle is directly established. When the tractor is under a non-pitching condition, the reference pitch angle of the lower link relative to the tractor body, $\theta_{b0}$, is defined as

$$\theta_{b0} = se + r \tag{20}$$

where $e$ denotes the digital sampling value measured by the angle sensor; $s$ denotes the proportional coefficient between the digital sampling value and the pitch angle of the lower link; and $r$ denotes the initial offset coefficient of the lower-link pitch angle. During actual ploughing operation, the tractor undergoes pitch variation. When the tractor has a

pitch angle of $\theta_t$, the actual pitch angle of the lower link relative to the ground, $\theta_b$, can be expressed as $\theta_{b0} + \theta_t$. Thus,

$$l_{G'E} = l_{GE} sin(se + r + \theta_t) \tag{21}$$

where $l_{GE}$ denotes the length of GE. The tillage-depth calculation model is then given as

$$h = Kcos(\theta_a - \theta_t) + Qsin(se + r + \theta_t) + Psin(\theta_c + \theta_p) + D \tag{22}$$

Affected by the variations in mechanical clearance, tractor sinkage, and other factors induced by field operating conditions, errors inevitably exist in the structural parameters of the above model. To compensate for these errors, model calibration coefficients are introduced as $K = k \cdot l_{OG}$, $Q = q \cdot l_{GE}$, $P = p \cdot l_{EH}$, and $D = -h_o + d$. These coefficients are jointly determined by the geometric structural parameters and compensation parameters. Among these, the structural parameters ($l_{OG}$, $l_{GE}$, $l_{EH}$, $\theta_a$, and $\theta_c$) are fixed by the hitch geometry and can be directly measured. The parameters used to compensate for model deviations under actual field conditions, including the lower-link pitch angle $se + r$, $k$, $q$, $p$, and $d$, can be obtained through experimental calibration.

The angle-dependent calibration model characterizes tillage depth variation equivalently as a univariate function of the lift arm angle. Its applicability hinges on the premise that the relative pitch angle between the tractor and the implement remains constant. In contrast, the distributed tillage depth model describes the spatial positional correlations of the relevant linkages involved in the formation of tillage depth. When the attitudes of the tractor and plough vary, or when the hitch system is adjusted, these disturbances are reflected in the model inputs through $\theta_t$, $\theta_p$, and $e$. As shown in Figure 9, the tillage depth $h$ is jointly determined by the reference height of the rear wheel axle center $h_o$, and the vertical projections O'G, G'E, and E'H of the linkages OG, GE, and EH, respectively. By measuring $\theta_t$, $\theta_p$, and $e$, the lengths of the projections O'G, G'E, and E'H can be determined, thereby enabling the calculation of tillage depth.

## 3. Results and Discussion

### *3.1. Calibration of the Tillage Depth Model*

The distributed tillage depth model requires calibration of the correlation between the lower-link angle and the digital sampling value of the lift arm angle sensor, as well as the attitude-related compensation coefficients. A model relating the digital sampling value $e$ of the lift arm angle to the lower-link pitch angle $\theta_b$ was established. During calibration, the tractor was kept in a horizontal state, and the lift arm was driven to perform reciprocating lifting and lowering motions through the three-point hitch system. An IMU was mounted on the lower link to acquire its real-time pitch angle, while an STM32 microcontroller was used to synchronously collect the digital sampling values of the lift arm angle and the pitch-angle data of the lower link. The fitted correlation between the two variables is shown in Figure 10.

The geometric structural parameters and compensation parameters in the distributed tillage depth model were experimentally calibrated. The geometric structural parameters, including $\theta_a$, $\theta_c$, OG, GE, EH, and $h_o$, are acquired by manual measurement. These parameters, alongside the corresponding calibration coefficients, are summarized in Table 4. Specifically, the tractor was driven to different positions on a slope, and the lift arm was adjusted to different angles. The microcontroller synchronously acquired tractor pitch angle, lift arm angle digital sampling values, and measured tillage depth. Least-squares fitting was subsequently applied to the collected dataset to estimate the compensation parameters. By combining the compensation parameters with the structural parameters, the final coefficients of the tillage depth model were determined.

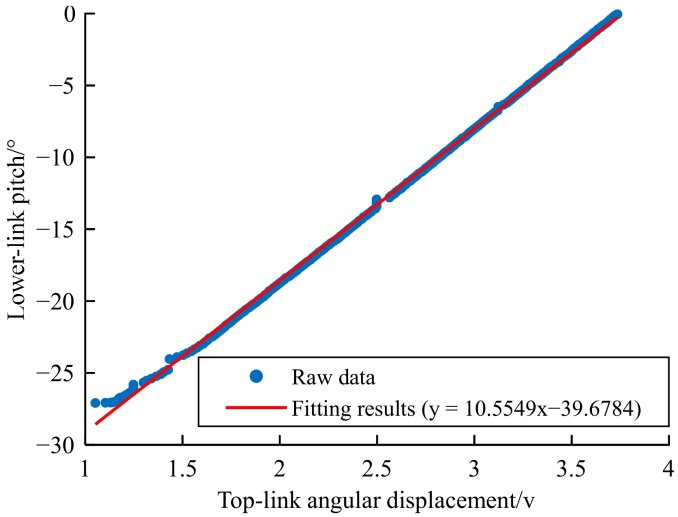



**Figure 10.** Correlation between AD value of top-link angular displacement and lower link pitch.

**Table 4.** Geometric structure parameters and distributed model coefficients.

| Name | Parameter | Value |
|---|---|---|
| Plough-frame angle | $\theta_a$ | 30° |
| Wheel-center hinge angle | $\theta_c$ | 16° |
| Wheel-center hinge length | $l_{OG}$ | 250 mm |
| Lower-link length | $l_{GE}$ | 912 mm |
| Plough-frame length | $l_{EH}$ | 2685 mm |
| Rear-wheel radius | $h_o$ | 750 mm |
| Tractor-body influence coefficient | $K$ | 212.775 |
| Hitch influence coefficient | $Q$ | 813.595 |
| Plough influence coefficient | $P$ | 2884.764 |
| Bias coefficient | $D$ | −773.451 |

By substituting the calibrated coefficients into (22), the distributed tillage depth model is expressed as follows:

$$H = 212.775cos(30° - \theta_t) + 813.595sin(10.554 \cdot e - 39.678 + \theta_t) + 2884.764sin(16° + \theta_p) - 773.451 \quad (23)$$

The calibration results of the model are shown in Figure 11. The root mean square error (RMSE) of the model was 10.1 mm, and the coefficient of determination $R^2$ was 0.997. In this context, a negative tillage depth indicates that the plough is located above the horizontal plane of the tractor rear wheel. It should be noted that dynamic fluctuations in tillage depth during field operations mainly stem from terrain irregularities and the longitudinal pitch motion of the tractor and coupled implement. In addition, the three-point hitch linkage lengths were repeatedly adjusted during plough assembly to guarantee the plough maintains optimal roll balance throughout field work.

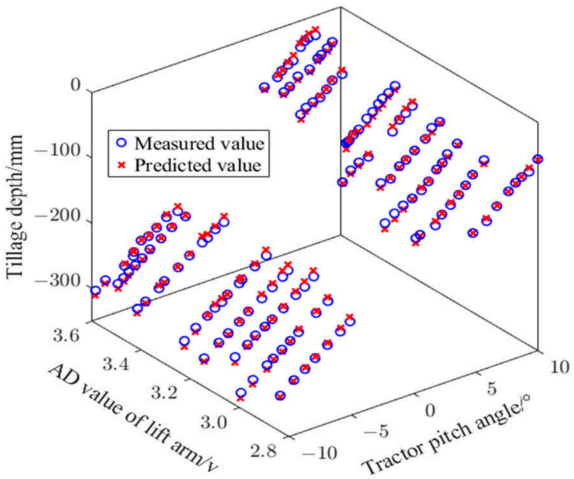



**Figure 11.** Results of distributed tillage depth model calibration.

### *3.2. Field Ploughing Experiment*

To validate the performance of the tillage-depth monitoring system based on dynamic attitude compensation under actual field operating conditions, field experiments were conducted at Runguo Farm in Zhenjiang, Jiangsu Province. The experimental scenario is shown in Figure 12. The test field was clay loam soil without crop-residue cover, and the operating speed was approximately 3.5–4.0 km/h. The tillage depth was measured using both the distributed tillage-depth model and ultrasonic ranging, and the corresponding data were recorded by the host computer for subsequent post-processing analysis.




**Figure 12.** Field test scenario. 1. Ultrasonic sensor, and 2. manually measured tillage depth.

In the field experiments, the reference tillage depth was obtained by combining ultrasonic ranging sensor data with the corresponding geometric correlation. Because of its favorable measurement precision and continuous sampling performance, ultrasonic sensors have been widely applied for acquiring tillage-depth information. The ultrasonic sensor utilized in this work is an industrial-grade sensor (YM7733, Shanghai Ledu Intelligent Technology Co. Ltd., Shanghai, China) featuring a measurement range of 0.1 to 0.5 m with a nominal accuracy of ±5 mm. Prior to field testing, static bench calibration was conducted against a laser distance meter to eliminate systematic bias via sensor offset registers. To minimize environmental noise in field operations, the test field was intentionally selected as clay loam soil prepared by rotary tillage and leveling, effectively eliminating scattering interference from crop residue and large soil clods. The probe was mounted on the left-front side of the plough frame facing the unploughed smooth surface, avoiding mud adhesion and mechanical vibration splash. The tillage depth data derived from ultrasonic measurements are presented in Figure 13. To verify the reliability of ultrasonic tillage depth detection, the measured depth data from the ultrasonic sensor were compared with manual

field measurement results. The RMSE, mean absolute error (MAE), and standard deviation (STD) were used as evaluation metrics, and the detailed statistical results are presented in Table 5. The statistical results indicate that the MAE of the ultrasonic detection results was 5.3 mm and the RMSE was 5.6 mm, demonstrating an overall stable error level.

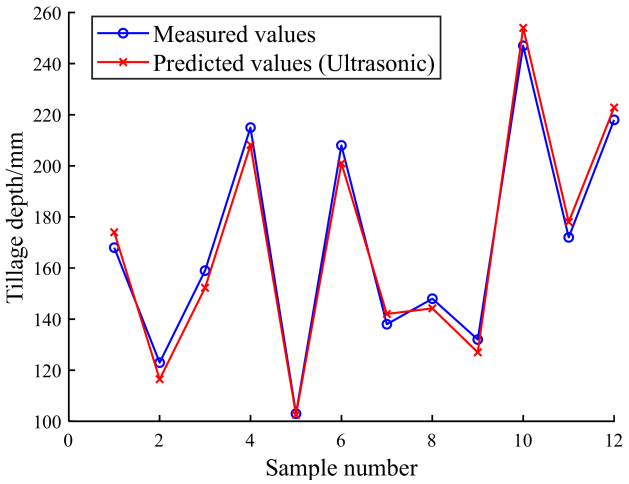



**Figure 13.** Results of ultrasonic-calculated tillage depth.

**Table 5.** Analysis of ultrasonic-calculated tillage depth.

| Name | RMSE (mm) | MAE (mm) | STD (mm) |
|---|---|---|---|
| Tillage depth | 5.6 | 5.3 | 5.7 |

Due to vibration of the tractor–implement unit and external acceleration disturbances during field operation, dynamic errors exist in the attitude measurements obtained from the IMU. In this study, the RKF was adopted to fuse the gyroscope and accelerometer data collected by the MEMS-IMU for attitude estimation. The attitude output from the MTi-300 attitude sensor was used as the reference, and both sensors operated at a sampling frequency of 100 Hz. The plough attitude results during field operation are shown in Figure 14 and Table 6. Compared with the conventional Kalman filter (KF), the RKF significantly improved the accuracy of attitude estimation, where the RMSE and MAE of pitch error are reduced by 21.3% and 18.4%.

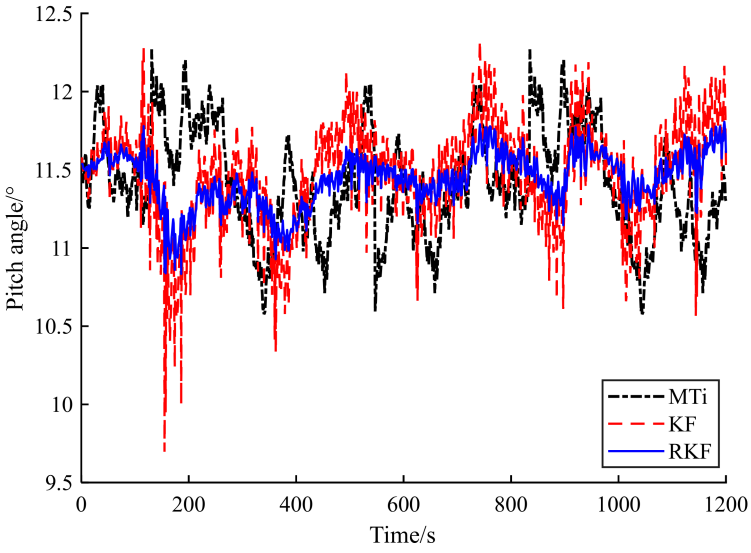



**Figure 14.** Result of plough attitude estimation.

**Table 6.** Results of pitch estimation for different algorithms.

| Algorithm | RMSE (°) | MAE (°) | STD (°) |
|---|---|---|---|
| KF | 0.47 | 0.38 | 0.47 |
| RKF | 0.37 | 0.31 | 0.37 |

To verify the detection accuracy of the proposed distributed tillage depth model, three comparative models are introduced for quantitative performance analysis in this section: the lift arm angle model (Model I), the lift arm angle model integrated with tractor pitch (Model II), and the lift arm angle model integrated with plough pitch compensation (Model III). The field experiments included two operating conditions, namely flat and bumpy farmland, with a total of eight continuous ploughing operations conducted. To intuitively demonstrate the dynamic detection performance under different disturbance conditions, two representative 10 s segments were selected from the experimental data for comparative analysis, as shown in Figure 15. The experimental results indicate that, under both flat and bumpy conditions, the proposed distributed tillage depth model can follow the reference tillage depth curve more accurately than the other models, thereby verifying the effectiveness and superiority of the proposed method in actual field ploughing operations. Under bumpy conditions, due to implement vibration, the measurement deviations of all the models relative to the ultrasonic reference values increased. However, the proposed model was less affected by disturbances and exhibited better consistency with the reference depth values.

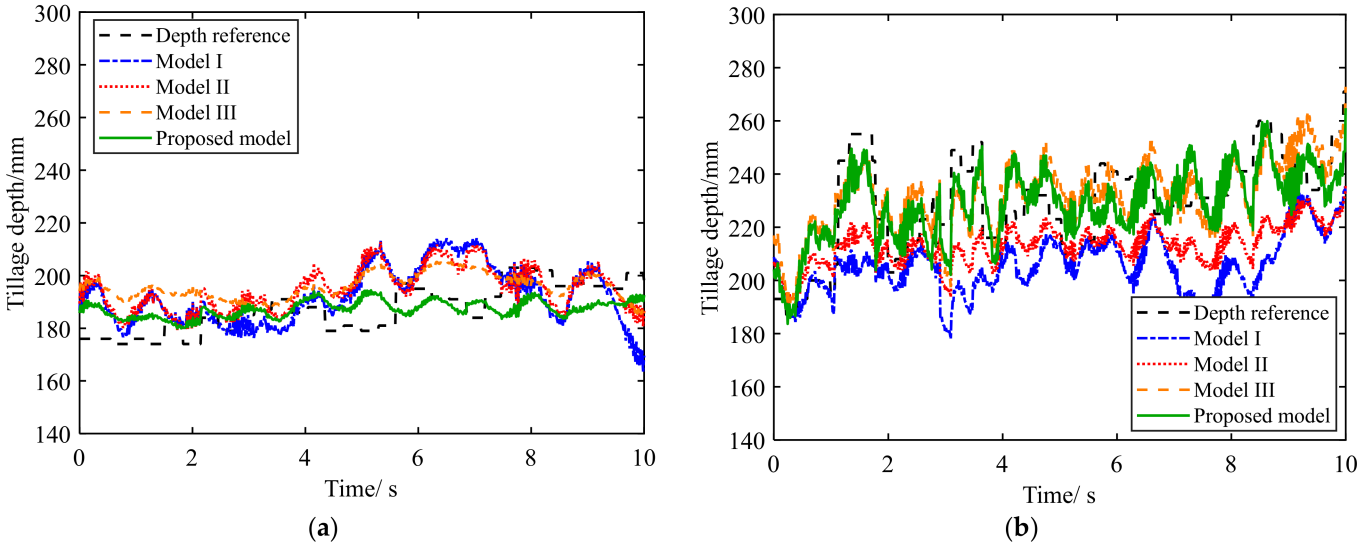



**Figure 15.** Results of different tillage depth models. (**a**) Flat farmland, and (**b**) bumpy farmland.

To further compare the performance and ablation contributions of the four tillage depth models, the statistical results of the tillage depth detection errors (RMSE, MAE, and STD) are given in Table 7. The proposed model outperforms the angle-based model and traditional pitch angle cascaded model under both operating conditions. Under flat conditions, the RMSE, MAE, and STD of the proposed model decreased by 23.0%, 13.6%, and 23.1%, respectively, compared with those of the lift arm angle model. Under bumpy conditions, the corresponding metrics decreased by 59.3%, 58.1%, and 25.7%, respectively. Compared with Model II, the proposed model reduces the RMSE, MAE, and STD by 23.0%, 12.6%, and 14.9% in flat conditions, and by 44.4%, 42.6%, and 11.4% in bumpy conditions. It is worth noting that Model III yields slightly better results for all performance metrics under bumpy conditions, while this trend is not observed during tillage on flat farmland. On flat

farmland, Model II and Model III cannot jointly incorporate pitch variations from the tractor and plough. They only slightly suppress depth errors of the angle-based model, especially for MAE and STD, while the RMSE of depth error exhibits no prominent improvement. In other words, these models boost stability without advancing tillage depth accuracy. By contrast, the proposed model achieves synchronous decoupling of dual-pitch components and optimizes detection accuracy and stability simultaneously.

**Table 7.** Results of tillage depth detection.

| Operating Scenarios | Data Sample | Proposed Model | | | Model I | | | Model II | | | Model III | | |
|---|---|---|---|---|---|---|---|---|---|---|---|---|---|
| | | RMSE | MAE | STD | RMSE | MAE | STD | RMSE | MAE | STD | RMSE | MAE | STD |
| Flat farmland | Data 1 | 8.1 | 7.0 | 8.0 | 12.7 | 9.9 | 12.0 | 12.9 | 10.1 | 10.2 | 12.8 | 10.0 | 10.3 |
| | Data 2 | 9.0 | 7.8 | 7.6 | 10.5 | 7.9 | 9.4 | 10.5 | 7.9 | 9.3 | 10.4 | 7.8 | 9.2 |
| | Data 3 | 8.5 | 7.3 | 8.5 | 11.8 | 9.4 | 11.0 | 11.4 | 9.1 | 9.5 | 11.3 | 9.0 | 9.4 |
| | Data 4 | 9.2 | 8.3 | 7.8 | 10.2 | 7.8 | 9.2 | 10.2 | 7.8 | 8.6 | 10.1 | 7.7 | 8.5 |
| | Average | 8.7 | 7.6 | 8.0 | 11.3 | 8.8 | 10.4 | 11.3 | 8.7 | 9.4 | 11.0 | 8.6 | 9.4 |
| Bumpy farmland | Data 5 | 12.0 | 10.3 | 12.0 | 27.4 | 22.9 | 15.7 | 19.9 | 16.7 | 12.9 | 18.8 | 15.6 | 12.5 |
| | Data 6 | 12.4 | 10.7 | 12.2 | 31.3 | 26.8 | 16.3 | 22.8 | 19.3 | 13.3 | 21.5 | 18.1 | 13.0 |
| | Data 7 | 12.7 | 11.1 | 12.7 | 30.8 | 25.4 | 18.0 | 22.9 | 19.0 | 15.4 | 21.8 | 18.2 | 14.8 |
| | Data 8 | 12.9 | 11.3 | 12.6 | 33.2 | 28.7 | 16.8 | 24.5 | 21.0 | 14.3 | 23.2 | 20.1 | 13.9 |
| | Average | 12.5 | 10.9 | 12.4 | 30.7 | 26.0 | 16.7 | 22.5 | 19.0 | 14.0 | 21.3 | 18.0 | 13.6 |

Terrain undulations and working unit vibrations change the relative pitch attitude of the tractor–plough system. Traditional angle-dependent detection methods fail to eliminate tillage depth errors originating from tractor pitch deflection, thus yielding low tillage depth detection precision. Although existing pitch-angle cascaded models are capable of counteracting tillage depth deviations caused by tractor pitch motion, they remain susceptible to interference stemming from tractor rear wheel sinkage and pitch fluctuations of the plough. The proposed distributed tillage depth model achieves precise calculation of relative pitch angles via anti-interference attitude estimation, and compensates terrain-induced tillage depth errors effectively. These results demonstrate that the distributed model effectively improves both the accuracy and disturbance rejection capability of tillage depth detection. Overall, the proposed model presents working stability and terrain adaptability, which satisfies the requirement for online real-time evaluation of tillage depth uniformity coefficients in field tillage operations.

## 4. Conclusions

In this study, a tillage depth detection method based on distributed attitude measurement is proposed to address the defects of indirect rotation angle-based models exposed under terrain undulation and vibration conditions, and reduce the sensitivity of tillage depth detection to structural adjustments of the three-point hitch. Experimental results confirm that converting three-point hitch structural variations into relative pitch angle offsets between the tractor and plough is a technically viable approach for mitigating terrain-induced tillage depth errors. Compared with the traditional angle-dependent tillage depth model and the existing tractor pitch angle cascaded compensation model, the proposed method delivers higher detection accuracy and superior terrain adaptability.

Nevertheless, this research still has certain limitations. First, all field experiments were carried out merely on clay loam soils with a mounted moldboard plough due to restricted experimental conditions. Although pitch is the primary governing variable for tillage depth in flatland ploughing, roll tilt induced by uneven terrain was not incorporated into the planar geometric model. In future work, we will extend the linkage kinematic derivation into a 3D spatial model with full attitude compensation to further enhance detection

accuracy during cross-slope operations. Subsequent research will also focus on expanding field tests across diverse soil types and complex operating conditions to comprehensively validate the universality and working adaptability of the proposed method. In addition, high-frequency random noise exists in the output of the established tillage depth model, which is mainly triggered by original noise interference from attitude sensors. Therefore, emerging techniques such as deep learning-based denoising algorithms will be adopted to suppress random sensor noise in our follow-up research, with the goal of further improving the output stability of the tillage depth prediction model.

**Author Contributions:** Conceptualization, B.C.; methodology, B.C. and Z.Y.; software, B.C. and Z.Y.; validation, Y.Z. and Z.H.; formal analysis, Y.Z.; investigation, Z.Y.; resources, Z.M.; data curation, Z.H.; writing—original draft preparation, Z.H. and B.C.; writing—review and editing, B.C. and Z.Y.; visualization, Y.Z.; supervision, B.C.; project administration, B.C.; funding acquisition, B.C. All authors have read and agreed to the published version of the manuscript.

**Funding:** This research was jointly funded by the National Natural Science Foundation of China, grant numbers 32271999 and 32401719; the Jiangsu Provincial Special Program for Frontier Technology Research (Modern Agriculture), grant number BF2025312; the Natural Science Foundation of Jiangsu Province, grant number BK20240877; the Youth Science and Technology Talent Support Project of Zhenjiang City, grant number ZJTJ-2025-021; and the Priority Academic Program Development of Jiangsu Higher Education Institutions, grant number PAPD-2023-87. The APC was funded by PAPD-2023-87.

**Data Availability Statement:** The data presented in this study are available on request from the corresponding author.

**Conflicts of Interest:** The authors declare no conflicts of interest.

## References

1. Zhai, Z.; Li, Y.; Guo, J.; Wang, J.; Dong, G.; Guo, Z.; Pang, H. Effects of tillage depth on soil physical properties and wheat-maize yield. *Trans. Chin. Soc. Agric. Eng.* **2017**, *33*, 115–123. [CrossRef]
2. Zhang, B.; Bai, T.; Wu, G.; Wang, H.; Zhu, Q.; Zhang, G.; Meng, Z.; Wen, C. Fatigue analysis of shovel body based on tractor subsoiling operation measured data. *Agriculture* **2024**, *14*, 1604. [CrossRef]
3. Zhu, Z.; Yang, Y.; Wang, D.; Cai, Y.; Lai, L. Energy Saving Performance of Agricultural Tractor Equipped with Mechanic-Electronic-Hydraulic Powertrain System. *Agriculture* **2022**, *12*, 436. [CrossRef]
4. Gao, J.; Qi, H. Soil throwing experiments for reverse rotary tillage at various depths, travel speeds, and rotational speeds. *Trans. ASABE* **2017**, *60*, 1113–1121. [CrossRef]
5. Ali Chandio, F.; Li, Y.; Xu, L.; Ma, Z.; Ahmad, F.; Minh Cuong, D.; Ali Lakhiar, I. Predicting 3D Forces of Disc Tool and Soil Disturbance Area Using Fuzzy Logic Model under Sensor Based Soil-Bin. *Int. J. Agric. Biol. Eng.* **2020**, *13*, 77–84. [CrossRef]
6. Liu, J.; Xia, C.; Jiang, D.; Sun, Y. Development and Testing of the Power Transmission System of a Crawler Electric Tractor for Greenhouses. *Appl. Eng. Agric.* **2020**, *36*, 797–805. [CrossRef]
7. Yu, Y.; Hao, S.; Guo, S.; Tang, Z.; Chen, S. Motor Torque Distribution Strategy for Different Tillage Modes of Agricultural Electric Tractors. *Agriculture* **2022**, *12*, 1373. [CrossRef]
8. Zhao, Z.; Li, H.C.; Liu, J.K.; Yang, S.X. Control method of seedbed compactness based on fragment soil compaction dynamic characteristics. *Soil Till. Res.* **2020**, *198*, 104551. [CrossRef]
9. Gao, Y.; Yang, Y.; Fu, S.; Feng, K.; Han, X.; Hu, Y.; Zhu, Q.; Wei, X. Analysis of Vibration Characteristics of Tractor–Rotary Cultivator Combination Based on Time Domain and Frequency Domain. *Agriculture* **2024**, *14*, 1139. [CrossRef]
10. Gao, Y.; Hu, Y.; Yang, S.; Zhao, X.; Lu, S.; Dou, H.; Zhu, Q.; Li, P.; Zhu, Y. Experimental Investigation of Impact Mechanisms of Seeding Quality for Ridge-Clearing No-Till Seeder Under Strip Tillage. *Agronomy* **2025**, *15*, 1875. [CrossRef]
11. Lu, E.; Xue, J.; Chen, T.; Jiang, S. Robust Trajectory Tracking Control of an Autonomous Tractor-Trailer Considering Model Parameter Uncertainties and Disturbances. *Agriculture* **2023**, *13*, 869. [CrossRef]
12. Han, J.; Yan, X.; Tang, H. Method of Controlling Tillage Depth for Agricultural Tractors Considering Engine Load Characteristics. *Biosyst. Eng.* **2023**, *227*, 95–106. [CrossRef]

13. Kim, Y.-S.; Kim, W.-S.; Siddique, M.A.A.; Baek, S.-Y.; Baek, S.-M.; Cheon, S.-H.; Lee, S.-D.; Lee, K.-H.; Hong, D.-H.; Park, S.-U.; et al. Power transmission efficiency analysis of 42kW power agricultural tractor according to tillage depth during moldboard plowing. *Agronomy* **2020**, *10*, 1263. [CrossRef]
14. Deng, Y.; Zhang, W.; Qi, B.; Wang, Y.; Ding, Y.; Zhang, H. Research Progress and Prospects of Intelligent Measurement and Control Technology for Tillage Depth in Subsoiling Operations. *Sensors* **2025**, *25*, 3821. [CrossRef] [PubMed]
15. Zhu, Y.; Cui, B.; Yu, Z.; Gao, Y.; Wei, X. Tillage Depth Detection and Control Based on Attitude Estimation and Online Calibration of Model Parameters. *Agriculture* **2024**, *14*, 2130. [CrossRef]
16. Tao, W.; Chen, B.; Yang, X.; Guo, B.; Xu, W.; Ke, S.; Huang, S. Design and Experimental Study of Tillage Depth Control System for Electric Rotary Tiller Based on LADRC. *Sci. Rep.* **2025**, *15*, 1740. [CrossRef] [PubMed]
17. Jia, H.; Guo, M.; Yu, H.; Li, Y.; Feng, X.; Zhao, J.; Qi, J. An Adaptable Tillage Depth Monitoring System for Tillage Machine. *Biosyst. Eng.* **2016**, *151*, 187–199. [CrossRef]
18. Kim, Y.-S.; Siddique, M.A.A.; Kim, W.-S.; Kim, Y.-J.; Park, S.-U.; Choi, C.-H. DEM simulation for draft force prediction of moldboard plow according to the tillage depth in cohesive soil. *Comput. Electron. Agric.* **2021**, *189*, 106368. [CrossRef]
19. Soylu, S.; Çarman, K. Fuzzy Logic Based Automatic Slip Control System for Agricultural Tractors. *J. Terramechanics* **2021**, *95*, 25–32. [CrossRef]
20. Sukcharoenvipharat, W.; Phoonkhwan, R.; Usaborisut, P. A low-cost soil strength and subsoiling depth measuring system and soil mapping derived from field tests. *J. Saudi Soc. Agric. Sci.* **2023**, *22*, 139–148. [CrossRef]
21. Lou, S.; He, J.; Lu, C.; Liu, P.; Li, H.; Zhang, Z. A Tillage Depth Monitoring and Control System for the Independent Adjustment of Each Subsoiling Shovel. *Actuators* **2021**, *10*, 250. [CrossRef]
22. Wang, A.; Ji, X.; Zhu, Y.; Wang, Q.; Wei, X.; Zhang, S. Tillage Depth Regulation System via Depth Measurement Feedback and Composite Sliding Mode Control: A Field Comparison Validation Study. *Meas. Control* **2024**, *57*, 685–702. [CrossRef]
23. Ma, R.; Wei, L.; Zhao, B.; Zhou, L.; Liu, Y.; Xing, G. Research on rotary tillage depth detection system based on multi-sensor data fusion. *Trans. Chin. Soc. Agric. Eng.* **2024**, *55*, 52–64. [CrossRef]
24. Jiang, X.; Tong, J.; Ma, Y.; Li, J.; Wu, B.; Sun, J. Research on subsoiling depth detection device based on Kalman filtering fusion algorithm. *Trans. Chin. Soc. Agric. Eng.* **2020**, *51*, 53–60. [CrossRef]
25. Du, X.; Yang, X.; Pang, J.; Ji, J.; Jin, X.; Chen, L. Design and experiment of tillage depth monitoring system for mounted rotary cultivator. *Trans. Chin. Soc. Agric. Eng.* **2019**, *50*, 43–51. [CrossRef]
26. Yin, Y.; Wang, C.; Meng, Z.; Chen, J.; Guo, S.; Qin, W. Research on tillage depth detection method for mounted subsoiler. *Trans. Chin. Soc. Agric. Eng.* **2018**, *49*, 68–74. [CrossRef]
27. Xia, J.; Li, D.; Liu, G.; Cheng, J.; Zheng, K.; Luo, C. Research on electro-hydraulic monitoring and control system for tractor mounted tillage depth based on angle detection. *Trans. Chin. Soc. Agric. Eng.* **2021**, *52*, 386–395. [CrossRef]
28. Hu, K.; Zhang, W.; Qi, B.; Ji, Y. Tillage Depth Dynamic Monitoring and Precise Control System. *Meas. Control* **2025**, *58*, 394–403. [CrossRef]
29. Candan, B.; Soken, H.E. Robust Attitude Estimation Using IMU-only measurements. *IEEE Trans. Instrum. Meas.* **2021**, *70*, 1–9. [CrossRef]
30. Chen, J.; Cui, B.; Wei, X.; Zhu, Y.; Sun, Z.; Liu, Y. Robust attitude estimation for low-dynamic vehicles based on MEMS-IMU and external acceleration compensation. *Sensors* **2024**, *24*, 4623. [CrossRef] [PubMed]


**Disclaimer/Publisher's Note:** The statements, opinions and data contained in all publications are solely those of the individual author(s) and contributor(s) and not of MDPI and/or the editor(s). MDPI and/or the editor(s) disclaim responsibility for any injury to people or property resulting from any ideas, methods, instructions or products referred to in the content.